PHYSICAL REVIEW C **85**, 034301 (2012)

Multiple β^- decaying states in ^{194}Re: Shape evolution in neutron-rich osmium isotopes

N. Al-Dahan,[1,2] P. H. Regan,[2,*] Zs. Podolyák,[2] P. M. Walker,[2] N. Alkhomashi,[3] G. D. Dracoulis,[4] G. Farrelly,[2] J. Benlliure,[5] S. B. Pietri,[2,6] R. F. Casten,[7] P. D. Stevenson,[2] W. Gelletly,[2] S. J. Steer,[2] A. B. Garnsworthy,[2,8] E. Casarejos,[5,9] J. Gerl,[6] H. J. Wollersheim,[6] J. Grebosz,[10] M. Górska,[6] I. Kojouharov,[6] H. Schaffner,[6] A. Algora,[11,12] G. Benzoni,[13] A. Blazhev,[14] P. Boutachkov,[6] A. M. Bruce,[15] I. J. Cullen,[2] A. M. Denis Bacelar,[15] A. Y. Deo,[2] M. E. Estevez,[5] Y. Fujita,[16] R. Hoischen,[17] R. Kumar,[18] S. Lalkovski,[15] Z. Liu,[19] P. J. Mason,[2] C. Mihai,[20] F. Molina,[11] D. Mücher,[14] B. Rubio,[11] A. Tamii,[21] S. Tashenov,[6] J. J. Valiente-Dobón,[22] and P. J. Woods[19]

[1]*Department of Physics, College of Science, University of Kerbala, Kerbala, Iraq*
[2]*Department of Physics, University of Surrey, Guildford GU2 7XH, United Kingdom*
[3]*King Abdulaziz City for Science and Technology (KACST), P.O. Box 6086, Riyadh 11442, Saudi Arabia*
[4]*Department of Nuclear Physics, Australian National University, Canberra, ACT 0200, Australia*
[5]*Universidad de Santiago de Compostela, Santiago de Compostela, Spain*
[6]*GSI, Planckstrasse 1, D-64291 Darmstadt, Germany*
[7]*Wright Nuclear Structure Laboratory, Yale University, New Haven, Connecticut 06520-8120, USA*
[8]*TRIUMF, 4004 Wesbrook Mall, Vancouver, British Columbia, V6T 2A3, Canada*
[9]*University of Vigo, E-36310, Spain*
[10]*The Henryk Niewodniczànski Institute of Nuclear Physics, PL-31-342, Kraków, Poland*
[11]*IFIC, CSIC-Universidad de Valencia, 46071 Valencia, Spain*
[12]*Institute of Nuclear Research of the Hungarian Academy of Sciences, Debrecen, H-4001, Hungary*
[13]*INFN Sezione di Milano, I-20133 Milano, Italy*
[14]*Institut für Kernphysik, Universität zu Köln, 50937 Köln, Germany*
[15]*School of Environment and Technology, University of Brighton, Brighton BN2 4GJ, United Kingdom*
[16]*Department of Physics, Osaka University, Toyonaka, Osaka 560-0043, Japan*
[17]*Department of Physics, Lund University, S-22100 Lund, Sweden*
[18]*Inter-University Accelerator Centre, New Delhi 110067, India*
[19]*School of Physics and Astronomy, University of Edinburgh, Edinburgh EH9 3JZ, United Kingdom*
[20]*Horia Hulubei National Institute of Physics and Nuclear Engineering, R-76900 Bucharest, Romania*
[21]*Research Centre for Nuclear Physics, Osaka University, Ibaraki, Osaka 567-0047, Japan*
[22]*INFN-Laboratori Nazionali di Legnaro, 35020 Legnaro, Italy*

(Received 18 July 2011; revised manuscript received 5 October 2011; published 5 March 2012)

β decays from heavy, neutron-rich nuclei with $A \sim 190$ have been investigated following their production via the relativistic projectile fragmentation of an $E/A = 1$ GeV ^{208}Pb primary beam on a $\sim$2.5 g/cm^2 ^{9}Be target. The reaction products were separated and identified using the GSI FRagment Separator (FRS) and stopped in the RISING active stopper. γ decays were observed and correlated with these secondary ions on an event-by-event basis such that γ-ray transitions following from both internal (isomeric) and β decays were recorded. A number of discrete, β-delayed γ-ray transitions associated with β decays from ^{194}Re to excited states in ^{194}Os have been observed, including previously reported decays from the yrast $I^\pi = (6^+)$ state. Three previously unreported γ-ray transitions with energies 194, 349, and 554 keV are also identified; these transitions are associated with decays from higher spin states in ^{194}Os. The results of these investigations are compared with theoretical predictions from Nilsson multi-quasiparticle (MQP) calculations. Based on lifetime measurements and the observed feeding pattern to states in ^{194}Os, it is concluded that there are three β^--decaying states in ^{194}Re.

DOI: 10.1103/PhysRevC.85.034301 PACS number(s): 25.70.Mn, 21.60.−n, 27.80.+w, 29.30.Kv

I. INTRODUCTION

Neutron-rich nuclei with $A \sim 190$ show a wide variation of nuclear structural properties and are characterized by the presence of different ground-state shapes, for example prolate, oblate, triaxial/γ-soft, and spherical [1–3]. The lighter isotopes of elements in this region are prolate deformed in their ground states and with the addition of more and more neutrons the shape becomes oblate [4]. At the $N = 126$ closed shell, the nuclei become spherical [5,6].

The Os-Pt region is known to be structurally very complex [7–9] with evidence of oblate, γ-soft, and triaxial deformations. As such, it offers a sensitive testing ground for nuclear models [10,11]. The Os isotopes exhibit a transition between deformed and spherical nuclei with increasing neutron number [3,12]. These characteristics suggest that the study of the neutron-rich Os isotopes may help us to understand the interplay between complex nuclear excitation modes [12]. The nucleus ^{194}Os has two neutrons more than the heaviest stable Osmium isotope, ^{192}Os. The study of the low-lying energy spectrum of ^{194}Os helps to illuminate how nuclear shapes are changing approaching the phase/shape transition region [3,12] for Os isotopes.

*p.regan@surrey.ac.uk

TABLE I. Experimental parameter details for the FRS settings, centered on the transmissions of ^{190}Ta, ^{192}Ta and ^{194}Re, respectively.

Setting	$B\rho_1$ (Tm)	$B\rho_2$ (Tm)	S2 degrader Thickness (mg/cm^2)	S4 degrader Thickness (mg/cm^2)	Beam Intensity (ion/spill)	Spill Repetition (s)	Total Collection time (h)
^{190}Ta	13.08	9.59	5050	3320	10^8	20	62
^{192}Ta	13.23	9.75	5050	3450	10^9	15	66
^{194}Re	13.05	9.45	5050	3040	4×10^8	7	6

The projectile fragmentation technique provides opportunities to observe nuclei far from stability [13]. Fragmentation has proved to be an efficient tool for producing exotic nuclear species and when combined with high sensitivity γ-ray detection arrays, structural information can be gained for otherwise inaccessible nuclei [14–17]. The highest sensitivity is achieved with both isomeric and β-delayed γ-ray spectroscopy techniques. Information on the excited states in nuclei populated in this way can be obtained when only a few hundred nuclei of interest are produced [18,19].

The research presented in this paper involves the production and structural investigation of the most neutron-rich isotopes of the elements rhenium (Re, $Z = 75$) and osmium (Os, $Z = 76$) studied to date and the correlation of the decay of ^{194}Re nuclei with γ rays from transitions in the daughter ^{194}Os nuclei. These nuclei were produced in projectile fragmentation reactions and identified using the Fragment Separator (FRS) [20] at the GSI Laboratory in Darmstadt, Germany. The decays of these nuclei have been studied following both β- and isomer-delayed γ-ray spectroscopy using the RISING [20,21] γ-ray spectrometer. The β-delayed studies utilized the RISING active stopper which enabled positional and temporal correlations to be determined between the implantation of a specific exotic isotope and its subsequent β decay. Some results from this same experiment on the decay of tantalum isotopes have been reported in Ref. [22].

II. EXPERIMENTAL DETAILS

The nuclei of interest were produced following the interaction of a ^{208}Pb primary beam with an energy of 1 GeV per nucleon from the SIS-18 synchrotron at GSI, with a ^{9}Be target of thickness 2.54 g/cm^2 located at the entrance of the FRS. The typical length of the primary beam spill was about 1 s.

To maximize the number of fully stripped ($q = Z$) nuclei passing through the FRS, niobium foils of 223 mg/cm^2 and 108 mg/cm^2 thicknesses were placed after the target and the degrader at the intermediate focal plane (S2). Three FRS settings are discussed in the current work, namely those centered on the transmission of fully stripped ^{190}Ta, ^{192}Ta and ^{194}Re ions. Note, that unless stated otherwise, the results shown in this work are from the summed data from the three settings outlined in Table I.

In this experiment the active stopper consisted of three 5×5 cm double-sided silicon strip detectors (DSSSDs; see Refs. [23,24]), each with 16 individual strips on the front and back faces. Figure 1 shows a schematic of the detector configuration at the final focal plane of the FRS at GSI which was used in this work.

The active stopper was viewed by the stopped RISING γ-ray spectrometer, which consists of 15 seven-element germanium cluster detectors with a measured full-energy peak efficiency of ~15% at 661 keV [25]. In the experiment described in this work, the active stopper [23] was used for the first time in conjunction with the RISING γ-ray array. The ions of interest were implanted in the active stopper detector setup. This highly pixellated silicon detector stack allows for correlation in time and space of the signal from the implanted ion and subsequent signals produced by β decays.

The technique of correlating the implanted ions with their subsequent β decay is based on the measurement of two main parameters: (i) the identification of the implantation position in the DSSSD detectors and (ii) the correlation time between the implanted ions and subsequent β particle detected in the same or any of eight neighboring pixels. In the current experiment, the FRS was operated in a monochromatic mode using an aluminium wedge-shaped degrader [20,26] at the intermediate focal plane (S2), which had the effect of distributing the implanted ions across a relatively wide area on the DSSSDs.

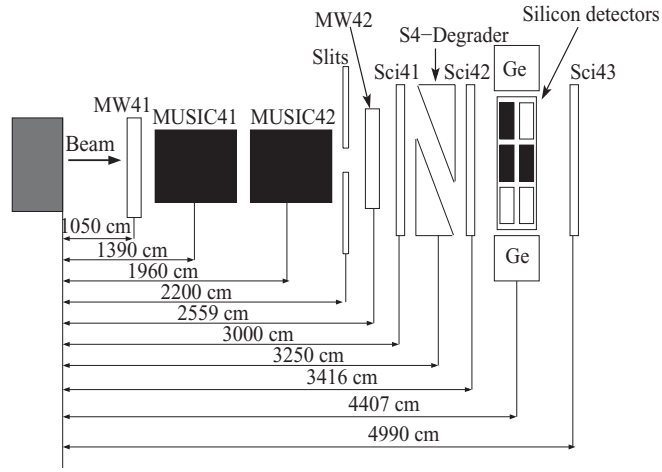

FIG. 1. Schematic of the detector configuration at the final focal plane of the FRS used in the present work, for the March 2007 experiment. Three of the possible six positions (black boxes) in the active stopper were occupied by DSSSDs in this particular experiment. MW = MultiWire detectors; Sci = Scintillator detectors; MUSIC = MUlti Sampling Ionizing Chamber detectors. The secondary ions were transmitted from left to right in this figure. The label "4" indicates that the detectors are placed at the final focal plane of the FRS.

This approach has two advantages; firstly it minimizes the probability of having multiple implantations in the same pixel during a typical correlation time; and second it minimizes the distribution range of the ions of a given species within the active stopper. Thus selected isotopes were stopped in a single layer in the active stopper silicon detectors. The ions were implanted in the active stopper and their positions determined by measuring the implantation strip positions as (x, y) coordinates. The absolute measurement of the implantation time was made with a digital, (absolute) time stamp. Valid implanted events were identified by the production of a high-energy signal in the active stopper detector (>10 MeV) measured using the logarithmic part of the preamplifier response. For the isomer measurements, the implant-γ-ray correlation time for the γ-ray electronic digital gamma finder (DGF) modules was fixed to be between $0 \rightarrow 400$ μs. After this time the γ-ray DGF electronics were closed for that event. If a subsequent decay signal was detected in the DSSSD, the decay trigger logic gave a signal for the γ-ray electronics to be opened again. For such events, the DGF electronics were opened for a further 400 μs period following the β trigger. To measure the β-decay signal, the linear region of the DSSSD preamplifiers was used. For each pixel where an implant occurred and for a specific period of time after the implantation, the energy deposited above the threshold (150 keV [23]) was considered to arise from the emission of a β particle from the radioactive ion implanted in the same pixel. Due to the finite β range in the DSSSDs and to increase the efficiency of measuring ion-correlated β-particle decay events in the off-line software analysis, a matching program was developed to record the decays in the pixels directly neighboring that of the original ion implant. Therefore, the correlation algorithm considered implantations and decays in the same pixel and decays in the eight directly neighboring pixels (i.e., the β particles were not always measured in the same pixel as the one where their radioactive mother ion was implanted). Each subsequent β^- particle in the same pixel could also be correlated in the time regime, until the implantation of a new ion. The average ion-implantation rate across the full DSSSD implantation array (i.e., across all pixels) was between 0.2 and 0.3 ions per second.

In this work, the β-delayed γ-ray spectroscopy of the ^{194}Re $\rightarrow$ ^{194}Os decay is discussed. The difference between applying the ion-β correlation only between (i) the implantations and decays in the same pixel and (ii) decays in the same pixel plus the eight neighboring pixels for the β-delayed γ-ray spectrum for the ^{194}Re decay is shown in Fig. 2. Panel (b) of Fig. 2 has poorer statistics but a better signal-to-noise ratio than the spectrum in panel (a). For this reason, the correlation algorithm applied subsequently to these data was only between the implantations and decays in the same pixel in the DSSSDs. This approach was applied to all β-delayed γ-ray spectra for the nuclei in the particle identification plot. To confirm this approach, good agreement was obtained from the comparison between the β-delayed γ-ray spectrum for excited states in ^{190}W from the current work with the previously reported results for this nucleus from isomer spectroscopy [27,28] as shown in Fig. 2(c). This result was published separately in Ref. [22].

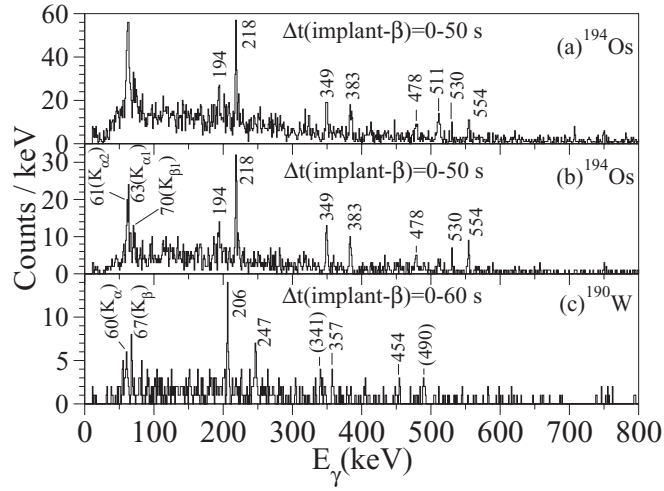

FIG. 2. (a) β-delayed γ-ray spectrum of ^{194}Os using the implantations and decays in the same pixel plus decays in any of the eight neighboring pixels; (b) β-delayed γ-ray spectrum of ^{194}Os using the implantations and decays in the same pixel and (c) shows the β-delayed γ-ray spectrum for excited states of ^{190}W to confirm the approach of using implantations and decays in the same pixel. This decay has been reported separately in Ref. [22].

A. Particle identification

The particle identifications in the current work were made on an event-by-event basis. There are two stages for the particle identification of the heavy ions in this type of study. The first step is a selection on in-flight changes in charge state. The FRS selection is dependent on the charge-changing properties of each ion as it passes through the detector and degrader materials of the FRS. "Fully stripped" ions correspond to no charge state change between the first and second sections of the FRS ($\triangle q = 0$), while "hydrogen-like" ions correspond to the pickup of one electron at the intermediate focal plane ($\triangle q = -1$), and "helium-like" ions correspond to the pickup of two electrons ($\triangle q = -2$). Charge state selection was achieved by using the position of the ion in plastic scintillators at the intermediate and final focal plane of the FRS to define the velocities and magnetic rigidities of the secondary ions. The difference in magnetic rigidity between the first and second stage of the fragment separator can be used to estimate the energy loss of the ion through the degrader. This information together with the energy loss of the ions as measured at the final focal plane using the MUSIC detectors allows a degree of charge state discrimination. This technique is of particular use in the case of heavy neutron-rich nuclei (see Refs. [29,30] for more details). For the separation of different charge states, it is necessary to derive how A/q and $B\rho$ depend on each other.

According to the charge state calculations using the GLOBAL code [31], 95.4% of the ^{194}Re ions were fully stripped exiting the target and 83.6% after the intermediate focal plane. For the FRS settings centered on the transmission of ^{190}Ta, ^{192}Ta, and ^{194}Re, the identification of the three charge state groups is shown in Fig. 3

The mass-to-charge ratio of the ions, (A/q), was determined from their time-of-flight (TOF) and magnetic rigidity measurements in the second part of the FRS. The TOF in the

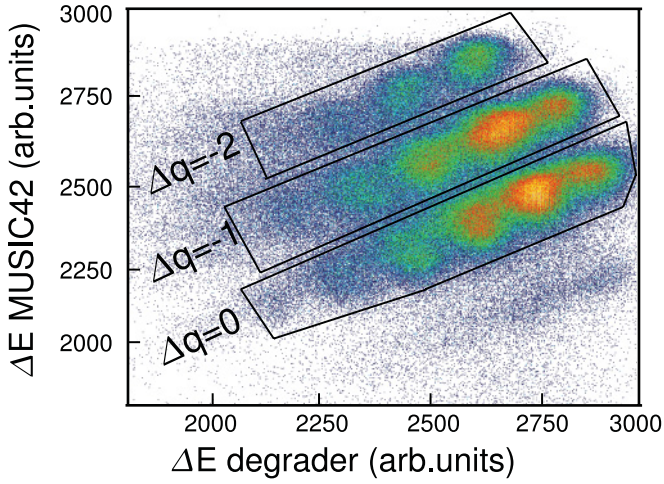

FIG. 3. (Color online) Charge state selection plot of nuclei centered on the transmission of fully stripped ions from summed data, using monochromatic mode.

second stage of the FRS was determined by measuring the time difference of the ions as they passed between two plastic scintillators which were placed (i) before the S2 degrader and (ii) at the final focal plane of the FRS. The change in the magnetic rigidity of ions was measured before and after they passed through the degrader at S2 which was used to obtain information on any change in charge state. The energy deposited by the identified fragments, which gives information on the atomic number (Z), was measured as they passed through two multisampling ionization chambers (MUSIC). By determining A/q, the charge state change, the position at the final focal plane and Z, an unambiguous event-by-event identification can be obtained. Further details of the particle identification technique are given in Refs. [6,32–34]. The transmitted ions were slowed down in a variable thickness aluminium degrader at the final focal plane and finally implanted into the active stopper. Figure 4 presents the particle identification plot for the summed data assuming fully stripped

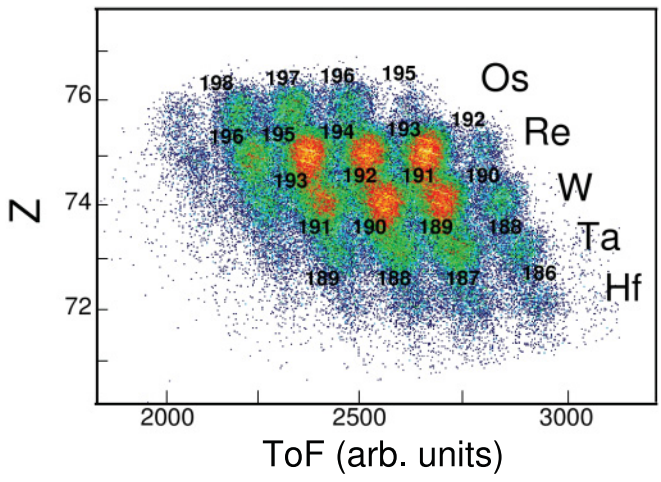

FIG. 4. (Color online) Particle identification plot for the summed data from the ^{190}Ta, ^{192}Ta, and ^{194}Re centered settings for fully stripped ions ($\triangle q = 0$).

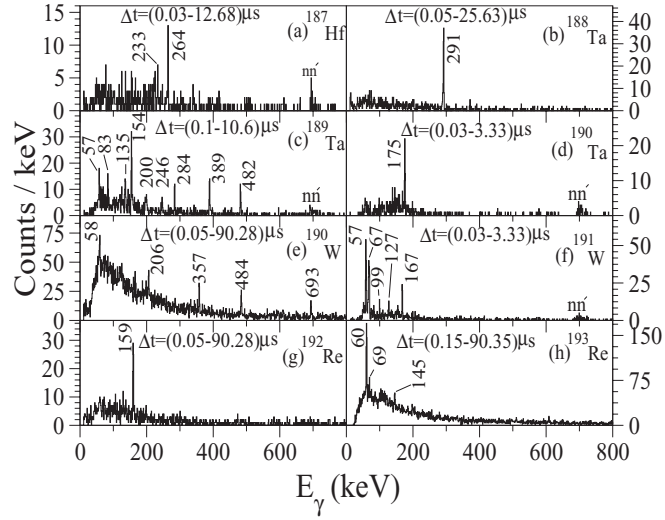

FIG. 5. γ-ray spectra from isomeric decays in (a) ^{187}Hf for a time range $\Delta t = (0.03 - 12.68)\mu$s, (b) ^{188}Ta for a time range $\Delta t = (0.05 - 25.63)\mu$s, (c) ^{189}Ta for a time range $\Delta t = (0.1 - 10.6)\mu$s, (d) ^{190}Ta for a time range $\Delta t = (0.03 - 3.33)\mu$s, (e) ^{190}W for a time range $\Delta t = (0.05 - 90.28)\mu$s, (f) ^{191}W for a time range $\Delta t = (0.03 - 3.33)\mu$s, (g) ^{192}Re for a time range $\Delta t = (0.05 - 90.28)\mu$s, and (h) ^{192}Re for a time range $\Delta t = (0.15 - 90.35)\mu$s, from the present work [16,22].

ions ($\triangle q = 0$). In this figure, the atomic number, Z, which is calculated from the energy loss of the ions in the MUSIC detector, is plotted versus the TOF in the second half of the FRS, which is related via the magnetic rigidity to the $\frac{A}{q}$ of the transmitted ions [30].

B. Confirming the ion identification

The secondary ions were separated, selected, and identified primarily using their A/q values. The ions were implanted in the three DSSSDs. The previously reported isomeric decays in ^{188}Ta [16], ^{190}W [27,28], ^{192}Re [16,35], and ^{193}Re [16,35] were all clearly identified as well as evidence for isomeric decays in ^{187}Hf, ^{189,190}Ta, and ^{191}W, reported previously in Ref. [22]. The particle identification procedure provided an independent validation for the γ-ray energy and timing setups. Figure 5 shows the final γ-ray energy spectra corresponding to decays from isomeric states which are identified in the summed data from the ^{190}Ta, ^{192}Ta, and ^{194}Re centered settings, for fully stripped ions.

III. RESULTS

γ rays emitted following the β^- decay of ^{194}Re ($Z = 75$) to excited states in the daughter nucleus ^{194}Os ($Z = 76$) were measured. The β-delayed γ-ray spectrum of ^{194}Os for ion-β correlation times (in the same pixel) of $\Delta t(\text{implant} - \beta) =$ 0–50 s is shown in Fig. 2(b). The previously reported decays from the yrast 2^+, 4^+, and 6^+ states in ^{194}Os with energies 218 [12,36,37], 383 [12,37], and 530 [37] keV together with the characteristic osmium $K_{\alpha1}$, $K_{\alpha2}$, and $K_{\beta1}$ x rays with energies

63, 61, and 71 keV, respectively, are clearly identified in this spectrum. A discrete γ-ray transition with energy 478 keV is also observed, consistent with the previously reported decay [12] from the $I^\pi = 0_2^+$ state in ^{194}Os. Three previously unreported transitions in ^{194}Os with energies 194, 349, and 554 keV are also observed. To verify that these three transitions are associated with decays in the ^{194}Os daughter nucleus, β^--delayed γ-ray spectra for all the nuclei in the particle identification plot of fully stripped ions from the summed data were examined for short [Δt(implant $-$ β) $= 0 \rightarrow 30$ s] and long [Δt(implant $-$ β) $= 0 \rightarrow 120$ s] correlation times. The γ-ray transitions with energies 194, 349, and 554 keV are only associated with the decay of ^{194}Re into ^{194}Os.

The decay half-lives of the mother nuclei were deduced from the time correlation between the implantation time of the identified fragments in the DSSSD detector and the subsequent β decay in the same pixel. The time correlation was determined using the same DGF time stamping system used in the isomer decay analysis, providing a resolution of 25 ns [23]. The time differences were histogrammed and used to generate a β decay curve for the identified fragments. These data could then also be further gated by the condition that specific discrete γ rays associated with decay in the daughter nuclei were also observed. The decay curves were fitted to single-component exponential decays using a least square fitting minimisation method and assuming a constant background level. Using the β^--correlation only approach, the half-life measurement for ^{192}Re of 16(2)s is consistent with the literature value for this decay of 16(1) s [38,39]. The decay time curves for both ^{192}Re and ^{194}Re from the current work for ion-β correlations are shown in Figs. 6(a) and 6(b), respectively, for the summed data from the ^{190}Ta, ^{192}Ta, and ^{194}Re centered settings.

^{194}Re is the heaviest isotope of this element studied to date. A single component exponential fit to the decay function for times between ion implantation and subsequent β^- decay in the same pixel for ^{194}Re ions is shown in Fig. 6. This simple

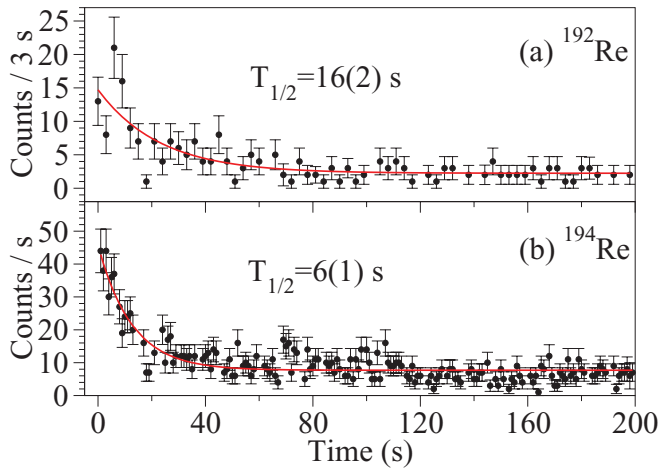

FIG. 6. (Color online) Decay time curve for β decay of (a) ^{192}Re and (b) ^{194}Re from ion-β time correlations for the summed data from the ^{190}Ta, ^{192}Ta, and ^{194}Re centered settings. By using a least squared fit the data were fitted to a single exponential decay function plus a constant background level.

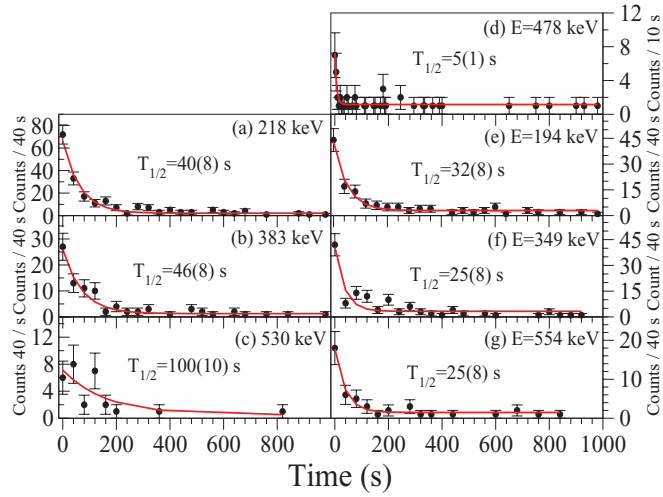

FIG. 7. (Color online) β-delayed γ-ray gated time spectra for the transitions 218, 383, 530, 478, 194, 349, and 554 keV associated with decay in ^{194}Os for different correlation times Δt(implant $-$ β) $= 0 \rightarrow 1000$ s from the current work. By using a least squared fit the data were fitted to a single exponential decay function plus a constant background level.

fitting procedure yields a fitted value for the apparent decay life for ^{194}Re of 6(1) s. However, it is important to note that this represents only pure ion-β correlation times, with no selection (via additional γ-ray gating) of which states were populated in the ^{194}Os daughter nucleus following the decay of the ^{194}Re mother.

The γ-ray gated β-decay time spectra associated with all the identified transitions in the β-delayed γ-ray spectrum of ^{194}Os were measured for different correlation times between Δt(implant $-$ β) $= 0 \rightarrow 1000$ s, see Fig. 7. These data are summarized in Table II and suggest that there are (at least) *three* separate β^- decaying states from ^{194}Re into ^{194}Os. The experimental arguments for this interpretation are outlined as follows. For the 530 keV transition [see Fig. 7(c)], there is intensity associated with the decay transition after 160 s while in the case of the 478 keV transition [see Fig. 7(d)], no such intensity is apparent above the constant, random background level after 40 s. The ^{194}Re decay half-life associated with feeding to the 478 keV transition was measured to be 5(1) s, consistent within the experimental uncertainties of the half-life value from the decay time for the pure ion-β correlation shown in Fig. 6(b). There is evidence for a decay with $T_{1/2} =$ 5(1) s [see Figs. 6(b) and 7(d)] which feeds the 0_2^+ state in ^{194}Os. Note that by the usual β decay selection rules, this also implies a significant degree of feeding in the β decay of ^{194}Re *direct to the* $I^\pi = 0^+$ *ground state* of ^{194}Os, which is not associated with any coincident, β-delayed γ-ray transition. This is consistent with the observation of a half-life of 6(1) s obtained in Fig. 6(b) for the correlations between ions and β particles only. A second decay with a half-life of approximately 25(8) s was measured from the β-delayed γ-ray projection gated by the 349 keV transition, see Fig. 7(f). There is also evidence for a third decaying state in ^{194}Re with a longer half-life of approximately 100 s which feeds the 6_1^+ state in ^{194}Os.

TABLE II. Experimental energies and relative intensities of γ-ray transitions identified in ^{194}Os following the decay of ^{194}Re as observed for implant$-(\beta^-\gamma)$ correlation times of $0 \rightarrow 10$ s, $0 \rightarrow 40$ s, and $40 \rightarrow 440$ s in the current work.

Correlation time [Δt (implant$-(\beta^- - \gamma)$]	$I_i \rightarrow I_f$	E_γ (keV)	I_γ relative
		193.4(3)	83(20)
	$2^+ \rightarrow 0^+$	218.3(4)	132(30)
		348.6(3)	75(20)
$0 \rightarrow 10$ s	$4^+ \rightarrow 2^+$	383.8(5)	40(15)
	$0_2^+ \rightarrow 2^+$	477.6(4)	70(24)
	$6^+ \rightarrow 4^+$	530.1(6)	18(18)
		554.1(2)	50(20)
		193.6(4)	87(23)
	$2^+ \rightarrow 0^+$	218.2(3)	214(37)
		349.0(3)	154(32)
$0 \rightarrow 40$ s	$4^+ \rightarrow 2^+$	383.3(4)	99(27)
	$0_2^+ \rightarrow 2^+$	477.8(5)	79(24)
	$6^+ \rightarrow 4^+$	530.1(6)	18(18)
		553.9(3)	94(27)
		193.6(3)	65(33)
	$2^+ \rightarrow 0^+$	218.2(2)	301(51)
		348.9(2)	187(38)
$40 \rightarrow 440$ s	$4^+ \rightarrow 2^+$	383.2(3)	163(43)
	$0_2^+ \rightarrow 2^+$	477.9(6)	68(40)
	$6^+ \rightarrow 4^+$	530.4(3)	97(55)
		553.9(3)	69(32)

The long half-life explains the "nonobservation" of the 530 keV transition for short correlation times in the β-delayed γ-ray spectrum of ^{194}Os, see Fig. 8. By investigating the difference in ion-β decay profiles gated on specific γ-ray transitions in the ^{194}Os daughter, information could be inferred which leads to the conclusion that there are at least two and probably three individual states in ^{194}Re which β^- decay, each with a different decay half-life.[1] The three previously unreported γ-ray transitions with energies 194, 349, and 554 keV have been independently related to transitions in associated with decays from high-spin states in ^{194}Os identified in studies of deep inelastic reactions by Dracoulis *et al.* [41]. Dracoulis *et al.* placed these transitions in a level scheme of ^{194}Os as decays from states with spins/parities $I^\pi \sim 10^- - 11^-$ [41]. Figure 9 shows the section of the partial experimental level scheme for ^{194}Os observed by Dracoulis *et al.* [41] of relevance to the present work.

The β^- decay half-life for ^{192}Re extracted from the ion-β correlations from the present work is 16(2) s. By contrast with the ^{194}Re decay case, the γ-gated spectrum associated with this decay shows no clear evidence of feeding in the current work to previously reported, low-lying states in ^{192}Os [42]. Figure 2(a) does show a small cluster of counts just below the expected energy of the yrast 2^+ state in ^{192}Os (206 keV), which might represent weak evidence for some (possibly indirect) feeding, the statistics are not sufficient in the current work to demonstrate a direct branch. The finite statistics obtained in the current work favours an interpretation of a single decaying state, probably of low-spin (0^+ or 0^-) which decays predominantly direct to the ground state of ^{192}Os.

[1]We are aware of recent results of mass measurements from the GSI Storage Ring that are consistent with ^{194}Re having two long-lived metastable states at excitation energies less than 1 MeV with lifetimes in the seconds range, in addition to the β^- decaying ground state [40].

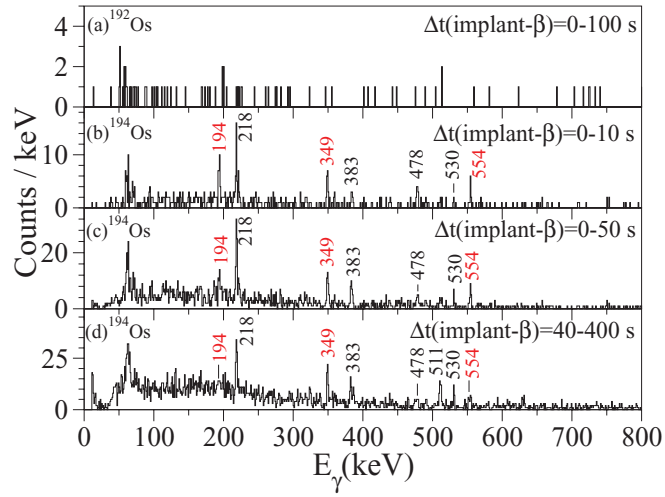

FIG. 8. (Color online) β-delayed γ-ray spectra showing transitions in (a) ^{192}Os for correlation time Δt(implant $- \beta$) $= 0 \rightarrow 100$ s from the decay of ^{192}Re. (b) ^{194}Os for correlation time Δt(implant $- \beta$) $= 0 \rightarrow 10$ s, (c) ^{194}Os for correlation time Δt(implant $- \beta$) $= 0 \rightarrow 50$ s, and (d) ^{194}Os for correlation time Δt(implant $- \beta$) $= 40 \rightarrow 400$ s, from the decay of ^{194}Re of fully stripped ions from the combination of ^{190}Ta, ^{192}Ta, and ^{194}Re settings. Previously unreported transitions are labeled in red.

IV. DISCUSSION

A. Multi-quasiparticle (MQP) calculations for ^{194}Re

Multi-quasiparticle (MQP) calculations have been performed to predict the spins and parities of the low-lying states in the ^{194}Re mother nucleus. These have been performed

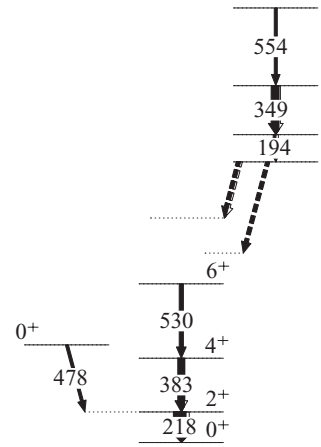

FIG. 9. Partial energy level scheme for ^{194}Os (from [44]) showing decay γ rays observed in the present work following the β^- decay of ^{194}Re.

TABLE III. Results of the multi-quasiparticle (MQP) calculations for the ^{194}Re mother nucleus of the spin and the parity of low-lying states in this nucleus for axially symmetric prolate and oblate deformations. The quadrupole (ε_2) and the hexadecapole (ε_4) deformation parameters are taken from Ref. [43] ($\varepsilon_2 = 0.125$, $\varepsilon_4 = 0.067$ for the prolate deformation).

Oblate						Prolate					
I^π	Neutron orbital (ν)	Proton orbital (π)	Energy[a] (keV)	V_R[b] (keV)	Net[c] (keV)	I^π	Neutron orbital (ν)	Proton orbital (π)	Energy[a] (keV)	V_R[b] (keV)	Net[c] (keV)
6^+	$3/2^-[501]\uparrow$	$9/2^-[514]\uparrow$	22		(22)	1^+	$1/2^+[660]\uparrow$	$1/2^+[411]\downarrow$	64	+70	134
3^+						0^+			64	−70	−6
7^+	$13/2^+[606]\uparrow$	$1/2^+[411]\downarrow$	91	+70	161	2^+	$1/2^+[660]\uparrow$	$3/2^+[402]\downarrow$	2	+70	72
6^+			91	−70	21	1^+			2	−70	−68
9^+	$13/2^+[606]\uparrow$	$5/2^+[402]\uparrow$	24	−84	−60	3^+	$3/2^+[651]\uparrow$	$3/2^+[402]\downarrow$	174	+70	244
4^+			24	+84	108	0^+			174	−70	104
10^+	$13/2^+[606]\uparrow$	$7/2^+[404]\downarrow$	337	+63	400	1^-	$1/2^+[660]\uparrow$	$1/2^-[550]\uparrow$	0	−70	−70
3^+			337	−63	274	0^-			0	+70	+70
2^-	$3/2^-[501]\uparrow$	$1/2^+[411]\downarrow$	67		(67)	2^-	$3/2^+[651]\uparrow$	$1/2^-[550]\uparrow$	173	−71	102
1^-						1^-			173	+71	244
4^-	$3/2^-[501]\uparrow$	$5/2^+[402]\uparrow$	0		(0)						
1^-											
5^-	$5/2^-[503]\downarrow$	$5/2^+[402]\uparrow$	264		(264)						
0^-											
11^-	$13/2^+[606]\uparrow$	$9/2^-[514]\uparrow$	46	−71	−25						
2^-			46	+71	117						
12^-	$13/2^+[606]\uparrow$	$11/2^-[505]\uparrow$	304	−71	233						
1^-			304	+71	375						

[a]Energy of the state.
[b]Empirical residual interactions.
[c]Sum of energy and V_R (keV).

for both the prolate and oblate deformations in this nucleus assuming axial symmetry, see Table III. The MQP calculations predict that in the case of the ^{194}Re nucleus there is a low-lying prolate configuration with $I^\pi = 11^-$, arising from the coupling of the neutron orbital $13/2^+[606]\uparrow$ to the proton orbital $9/2^-[514]\uparrow$. For oblate deformation, the lowest predicted energy states from these calculations have $I^\pi = 0^+$, 1^-, and 1^+ arising from the coupling of the neutron in the $1/2^+[660]\uparrow$ orbital with the $1/2^+[411]\downarrow$, $1/2^-[550]\uparrow$, and $3/2^+[402]\downarrow$ proton orbitals, respectively.

Assuming that there are three β-decaying components with three different half-lives from the ^{194}Re mother nucleus, from the half-life measurements one possibility is that an oblate, low spin (0^+, 1^-, or 1^+) state decays to the 0_1^+ and 0_2^+ states with a 5(1) s half-life [see Fig. 7(d)], while the predicted 11^- prolate state feeds the higher-spin sequence associated with the 194, 349, and 554 keV transitions. Evidence for a third β-decaying state comes from the longer apparent feeding time to the yrast 6^+ state in ^{194}Os. Note, if the prolate and oblate minima are based at the same energy, the MQP calculations predict 28 separate two-quasiparticle intrinsic states in ^{194}Re to lie below 400 keV, compared to just a single state in the even-even ^{194}Os daughter nucleus.

B. Low-lying collective structure of ^{194}Os

In the $A \sim 190$ region, for even-even Hf-Pt ($Z = 72 \rightarrow 78$) nuclei, the lighter isotopes are prolate deformed and as more and more neutrons are added the shape becomes oblate [1,2]. As the closed shell at $N = 126$ is approached, the shape of the nucleus is predicted to become spherical [5,6]. For the prolate-oblate transition region, the nuclei have a potential with similar energy minima corresponding to prolate and oblate shapes [17].

Hartree-Fock calculations with a Woods-Saxon single-particle potential, performed by Nazarewicz *et al.* [45], predict a ground-state oblate deformation for ^{194}Os with $\beta = -0.14$. The possibility of ^{194}Os having an oblate deformed ground state has also been proposed by Casten *et al.* [36]. The yrast states in ^{194}Os have been reported up to $I^\pi = (10^+)$ by Wheldon *et al.* using deep inelastic reactions [37]. The theoretical shape evolution with the number of nucleons for different chains of Yb, Hf, W, Os, and Pt isotopes for neutron number $N = 110 \rightarrow 122$ has also been studied by Sarriguren *at al.* [2] using Skyrme Hartree-Fock plus BCS approach. A signature for a transition from prolate to oblate shapes was predicted as the number of neutrons increases from $N = 110 \rightarrow 122$ for Os isotopes [2]. The lighter Os isotopes exhibit a rotational behavior which changes gradually toward γ soft as the number of neutrons increases [2]. The results by Sarriguren *et al.* [2] are supported by recent theoretical calculation using the same approach performed by Robledo *et al.* [3]. Their conclusion was that the prolate to oblate transition takes place at $N = 116$ [3] and that there is a tendency toward triaxial shapes as the proton number is increased for fixed neutron numbers [3]. The current results on the excited states in ^{194}Os can also be compared with

self-consistent, axially deformed Hartree-Fock calculations which have been performed for these nuclei [1,24,46] by using the Raman estimate [47], which relates the excitation energy of the first 2^+ state with the quadrupole deformation of the nucleus. The experimentally derived value of 218 keV for the first 2^+ state gives an estimate for the ground state deformation for ^{194}Os of $\beta_2 \sim 0.16$.

C. Systematics of ^{194}Os collective states

The energies of the lowest excited states can be used to infer information about the quadrupole character of the nuclei [48]. Systematics related to the yrast 2^+, 4^+, 6^+, the second 2^+ and 0^+ states [2_2^+ and 0_2^+)] as well as the calculated 6^+ states using the anharmonic vibrator model (AVM), ($6^+_{\text{Th.}}$) through the osmium isotopic chain are presented in Fig. 10. The energy of $6^+_{\text{Th.}}$ state was calculated by using the following relation:

$$6^+_{\text{Th.}} = \mathbf{(}3 \times E(2_1^+)\mathbf{)} + (3 \times \varepsilon), \tag{1}$$

where ε is calculated assuming the AVM using the following expression [49]:

$$\varepsilon = E(4_1^+) - \mathbf{(}2 \times E(2_1^+)\mathbf{)}, \tag{2}$$

where $E(2_1^+)$ and $E(4_1^+)$ are the excitation energies of the first 2^+ and 4^+ excited states, respectively. It is convenient to look at $\varepsilon/E(2_1^+)$. Clearly, for a harmonic vibrator, $\varepsilon/E(2_1^+) = 0$ while for a pure rigid axial rotor it is 4/3.

By using the $E(2_1^+)$ data, information about the collective character of the nuclei can be inferred. For the osmium isotopes, the yrast 2^+, 4^+, 6^+, and $6^+_{\text{Th.}}$ energies increase with increasing neutron number, N, while the excitation energy of the $I^\pi = 2_2^+$ decreases up to $N = 116$ and increases for heavier N values, as shown in Fig. 10. The excitation energy of the 0_2^+ states decreases from an energy of approximately 1 MeV in the $N = 110$ to 116 isotones ($^{184-192}$Os) and drops dramatically to approximately 700 keV in ^{194}Os, close in energy to the 2_2^+

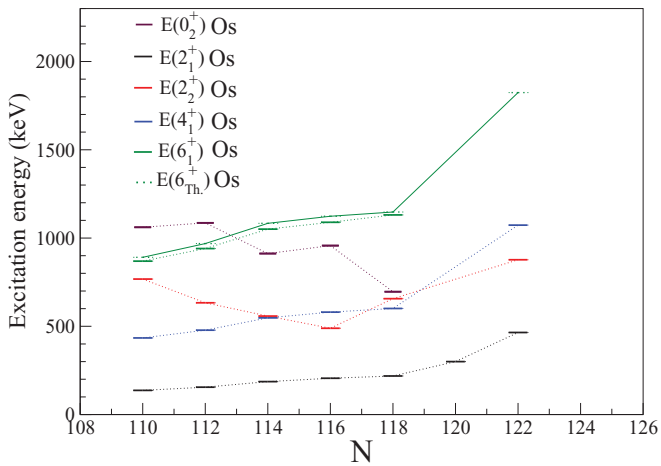

FIG. 10. (Color online) Systematics of the $E(2_1^+)$, $E(0_2^+)$, $E(2_2^+)$, $E(4_1^+)$, $E(6_1^+)$Exp, and $E(6_1^+)$Th. energies for the neutron number $N = 110$–122 for osmium isotopes.

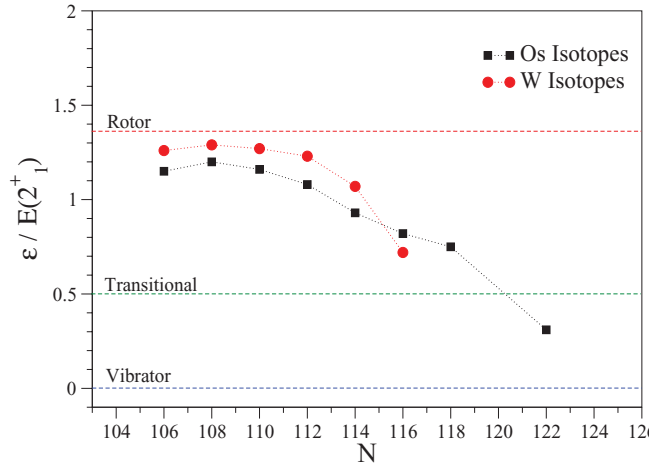

FIG. 11. (Color online) The ratio of the calculated anharmonicity ε values normalized to the excitation energy of the yrast state 2^+, $[\varepsilon/E(2_1^+)]$ for osmium isotopes with $N = 110$–122. [38].

and yrast 4^+ states. This gives rise to a near-energy triplet of 0_2^+, 2_2^+ and yrast 4^+ states in ^{194}Os which is consistent with a change in shape from the deformed γ-soft rotor observed for lighter Os isotopes, to a more quadrupole vibrational behavior at $N = 118$. The shape evolution in this region of the nuclear chart has been studied by Nomura *et al.* [4]. In particular, IBM calculations have been used to predict the energy sequence and transition rates in the osmium isotopes with increasing neutron number approaching $N = 120$ with parameters based on a mapping of predicted ground state deformations calculated using a Gogny energy density functional. These calculations predict a more γ-soft rotor behavior for ^{194}Os than is observed experimentally, with a higher-lying excited 0_2^+ state which is not reproduced by the experimental data. The ratio of $\varepsilon/E(2_1^+)$ decreases with N for both tungsten and osmium isotopes, see Fig. 11. As seen in the figure, $\varepsilon/E(2_1^+)$ has near rotor values for the light Os and W isotopes and decreases with increasing neutron number. For the heaviest isotopes known to date, it is passing through a transitional region, apparently en route toward vibrator values.

V. CONCLUSIONS

A number of discrete, β-delayed γ-ray transitions associated with β decays from ^{194}Re to excited states in ^{194}Os have been observed, including previously reported decays from the yrast $I^\pi = (6^+)$ state in this nucleus. Three previously unreported γ-ray transitions with energies 194, 349, and 554 keV are also identified. The results suggest that there are three separate β-decaying states in the ^{194}Re which feed the (1) 0_2^+ state and the 0^+ ground state of ^{194}Os with $T_{1/2} = 5(1)$ s; (2) (11^-) high-spin state in ^{194}Os [$T_{1/2} = 25(8)$ s]; (3) and possibly to the (6^+) yrast state in ^{194}Os [$T_{1/2} = 100(10)$ s].

Nilsson multi-quasiparticle calculations for prolate and oblate (axially symmetric) deformations predict a variety of possible low-lying candidate states in ^{194}Re which would be

expected to β decay to excited states in ^{194}Os. Specifically, both prolate (high-spin) and oblate (low-spin) configurations are predicted for ^{194}Re with spin/parities consistent with the expected decays which are observed to populate discrete levels in the ^{194}Os daughter nucleus. The excitation energy levels for states in ^{194}Os when compared with systematics for the Osmium isotopic chain are consistent with a γ-soft nucleus, as predicted by contemporary TRS and HF mean-field calculations for this nucleus.

ACKNOWLEDGMENTS

The excellent work of the GSI accelerator staff is acknowledged. This work is supported by the EPSRC(UK), STFC(UK), AWE plc, the Iraqi Government by Ministry of Higher Education and Scientific Research, University of Kerbala, College of Science, Department of Physics, The German BMBF under Grant No. 06KY205I, and the US DOE under grant No. DE-FG02-91ER-40609.

[1] P. D. Stevenson, M. P. Brine, Z. Podolyak, P. H. Regan, P. M. Walker, and J. R. Stone, Phys. Rev. C **72**, 047303 (2005).
[2] P. Sarriguren, R. Rodriguez-Guzmán, and L. M. Robledo, Phys. Rev. C **77**, 064322 (2008).
[3] L. M. Robledo, R. Rodríguez-Guzmán, and P. Sarriguren, J. Phys. G: Nucl. Part. Phys. **36**, 115104 (2009).
[4] K. Nomura, T. Otsuka, R. Rodríguez-Guzmán, L. M. Robledo, P. Sarriguren, P. H. Regan, P. D. Stevenson, and Z. Podolyák, Phys. Rev. C **83**, 054303 (2011).
[5] K. H. Maier *et al*., Phys. Rev. C **30**, 1702 (1984).
[6] S. J. Steer *et al*., Phys. Rev. C **78**, 061302(R) (2008).
[7] S. W. Yates *et al*., Nucl. Phys. A **222**, 301 (1974).
[8] R. D. Bagnel *et al*., Phys. Lett. B **66**, 129 (1977).
[9] F. T. Baker *et al*., Nucl. Phys. A **258**, 43 (1976).
[10] C. Y. Wu *et al*., Nucl. Phys. A **607**, 178 (1996).
[11] C. Wheldon, P. M. Walker, P. H. Regan, T. Saitoh, N. Hashimoto, G. Sletten, and F. R. Xu, Phys. Rev. C **59**, R2334 (1999).
[12] E. R. Flynn and D. G. Burke, Phys. Rev. C **17**, 501 (1978).
[13] H. Geissel, G. Münzenberg, and K. Riisager, Annu. Rev. Nucl. Part. Sci. **45**, 163 (1995).
[14] J. Benlliure *et al*., Nucl. Phys. A **660**, 87 (1999).
[15] K. Krumbholz *et al*., Z. Phys. A **351**, 11 (1995).
[16] M. Caamaño *et al*., Eur. Phys. J. A **23**, 201 (2005).
[17] Zs. Podolyák *et al*., Phys. Rev. C **79**, 031305(R) (2009).
[18] M. Pfützner *et al*., Phys. Lett. B **444**, 32 (1998).
[19] Zs. Podolyák *et al*., Euro. Phys. J. Special Topics **150**, 165 (2007).
[20] H. Geissel *et al*., Nucl. Instrum. Methods Phys. Res. B **70**, 286 (1992).
[21] M. Górska *et al*., Acta Phys. Pol. B **38**, 1219 (2007).
[22] N. Alkhomashi *et al*., Phys. Rev. C **80**, 064308 (2009).
[23] R. Kumar *et al*., Nucl. Instrum. Methods Phys. Res. A **598**, 754 (2009).
[24] P. H. Regan *et al*., Int. J. Mod. Phys. E **17**, 8 (2008).
[25] S. Pietri *et al*., Nucl. Instrum. Methods Phys. Res. B **261**, 1079 (2007).
[26] G. Münzenberg, Nucl. Instrum. Methods Phys. Res. B **70**, 265 (1992).
[27] Zs. Podolyák *et al*., Phys. Lett. B **491**, 225 (2000).
[28] G. F. Farrelly *et al*., Acta Phys. Pol. B **40**, 885 (2009).
[29] S. J. Steer *et al*., Acta Phys. Pol. B **38**, 1283 (2007).
[30] J. Benlliure *et al*., Nucl. Phys. A **674**, 578 (1999).
[31] C. Scheidenberger *et al*., Nucl. Instrum. Methods Phys. Res. B **142**, 441 (1998).
[32] P. H. Regan *et al*., Nucl. Phys. A **787**, 491 (2007).
[33] Zs. Podolyák *et al*., Phys. Lett. B **672**, 116 (2009).
[34] S. Pietri *et al*., Nucl. Instrum. Methods Phys. Res. B **261**, 1079 (2007).
[35] S. J. Steer *et al*., Int. J. Mod. Phys. E **18**, 1002 (2009).
[36] R. F. Casten *et al*., Phys. Lett. B **76**, 280 (1978).
[37] C. Wheldon *et al*., Phys. Rev. C **63**, 011304(R) (2000).
[38] [http://www.nndc.bnl.gov/chart/] Online database, National Nuclear Data Center, (site visited: March, 2010).
[39] C. M. Baglin, Nucl. Data Sheets **84**, 717 (1998).
[40] M. Reed, P. M. Walker *et al*. (to be published).
[41] G. D. Dracoulis *et al*. (to be published, 2011).
[42] C. Baglin *et al*., Nucl. Data Sheets **84**, 717 (1998).
[43] P. Möller *et al*., At. Data Nucl. Data Tables **59**, 185 (1995).
[44] G. D. Dracoulis (to be published, 2011).
[45] W. Nazarewicz, M. A. Riley, and J. D. Garrett, Nucl. Phys. A **512**, 61 (1990).
[46] E. B. Suckling and P. D. Stevenson (private communication, 2009).
[47] S. Raman, C. W. Nestor Jr., and P. Tikkanen, At. Data Nucl. Data Tables **78**, 1 (2001).
[48] R. F. Casten, *Nuclear Structure from a Simple Perspective* (Oxford Science Publications, Oxford/New York, 2000).
[49] N. V. Zamfir and R. F. Casten, Phys. Rev. Lett. **75**, 1280 (1995).